Space Weather

RESEARCH ARTICLE
10.1029/2019SW002362

Effects of GNSS Receiver Tuning on the PLL Tracking Jitter Estimation in the Presence of Ionospheric Scintillation

K. Guo, M. Aquino, and S. Vadakke Veettil

Nottingham Geospatial Institute, University of Nottingham, Nottingham, UK

Key Points:
- GNSS receiver PLL bandwidth and integration time tuning has a minor effect on scintillation indices and signal $C/N0$ calculation
- A decrease in the bandwidth will decrease the PLL thermal noise but increase phase scintillation induced tracking jitter
- The 1-s scintillation indices and tracking jitter successfully describe the signal distortions under scintillation

Correspondence to:
K. Guo,
kai.guo@nottingham.ac.uk

Citation:
Guo, K., Aquino, M., & Vadakke Veettil, S. (2020). Effects of GNSS receiver tuning on the PLL tracking jitter estimation in the presence of ionospheric scintillation. *Space Weather*, *18*, e2019SW002362. https://doi.org/10.1029/2019SW002362

Received 26 SEP 2019
Accepted 3 JUN 2020
Accepted article online 11 JUN 2020

©2020. The Authors.
This is an open access article under the terms of the Creative Commons Attribution License, which permits use, distribution and reproduction in any medium, provided the original work is properly cited.

Abstract Ionospheric scintillation is an interference characterized by rapid and random fluctuations in radio frequency signals when passing through irregularities in the ionosphere. It can severely degrade the performance of Global Navigation Satellite System (GNSS) receivers, thus increasing positioning errors. Receivers with different tracking loop bandwidths and coherent integration times perform differently under scintillation. This study investigates the effects of GNSS receiver tracking loop tuning on scintillation monitoring and Phase Locked Loop (PLL) tracking jitter estimation using simulated GNSS data. The variation of carrier to noise density ratio ($C/N0$) under scintillation with different tracking loop settings is also studied. The results show that receiver tuning has a minor effect on scintillation indices calculation. The levels of $C/N0$ are also similar for different PLL bandwidths and integration times. Additionally, the tracking jitter is estimated by theoretical equations and verified using the relationship with the PLL discriminator output noise, which is calculated using the post-correlation measurements. Novel approaches are further proposed to calculate 1-s scintillation index, which enables to compute the tracking jitter at a rate of 1 s. It is found that 1-s tracking jitter can successfully represent the signal fluctuations levels caused by scintillation. This work is valuable for developing scintillation sensitive tracking error models and is also of great significance for GNSS receiver design to mitigate scintillation effects.

1. Introduction

Ionospheric scintillation refers to the rapid and random fluctuations in radio frequency signal amplitude and phase. It occurs when signals traverse through ionospheric irregularities. The probability of scintillation occurrence is strongly related to solar and geomagnetic activity (Basu et al., 1988). Aarons (1982) suggested that scintillation is more frequent in equatorial regions and auroral to polar regions.

Scintillation is one of the most challenging error sources for Global Navigation Satellite System (GNSS). Because of scintillation, GNSS signals become noisier, thus receiver performance is degraded. The effects of scintillation on receiver take place notably at the tracking stage (Sreeja et al., 2011). On the one hand, the rapid fluctuations caused by scintillation in the incoming carrier phase will increase the Phase Locked Loop (PLL) tracking errors, which lead to a higher probability of cycle slip (Humphreys et al., 2010); when the increased tracking error exceeds the pull-in range of the discriminator, a loss of phase lock may occur (Kaplan & Hegarty, 2017). On the other hand, the amplitude fluctuations caused by scintillation may decrease the carrier to noise density ratio ($C/N0$); when it is lower than the receiver threshold, the Delay Locked Loop (DLL) will declare a loss of lock event, which causes signal loss. The increased probability of losing lock and a large tracking error will contribute to an increase in code and carrier phase measurement errors, leading to a degraded GNSS positioning accuracy (Guo, Aquino, Veettil, et al., 2019; Pi et al., 2017).

Much effort has been made to analyze and model the effects of ionospheric scintillation on GNSS receivers. Knight and Finn (1998) studied scintillation stochastic models and developed an approach to evaluate the scintillation effects on Global Positioning System (GPS). They pointed out that the levels of scintillation required to cause signal loss depends on the receiver tracking loop bandwidth, filter order, and discriminator type. In the study of Hegarty et al. (2001), a scintillation signal model was developed and GPS scintillation signals were generated. It was found that the typical noncoherent DLLs are relatively robust to signal fluctuations caused by scintillation, while PLLs are generally more susceptible to scintillation effects. To calculate the scintillation induced tracking error, Conker et al. (2003) proposed the PLL and the DLL tracking

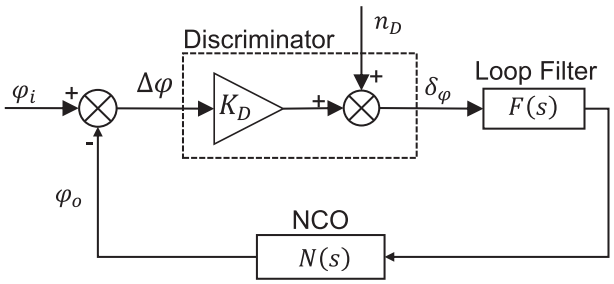

Figure 1. A simplified linear PLL tracking loop model.

error variance equations to calculate tracking errors caused by different error sources. The 1-min scintillation indices and 1-min averaged $C/N0$ were input to those equations in the study to evaluate the tracking error variances caused by scintillation. An extended model was developed by Moraes et al. (2014) to describe the effects of the scintillation on GPS receivers. By processing scintillation data recorded in Brazil, the tracking error variance was estimated and receiver performance was analyzed. Vadakke Veettil et al. (2018) built statistical models to estimate the standard deviation of the receiver PLL tracking errors as a function of scintillation levels exploiting the models in Conker et al. (2003) and Moraes et al. (2014) using the scintillation data recorded over 4 years at low and high latitudes. Guo, Aquino, and Vadakke (2019) analyzed the signal intensity fading due to scintillation. The results showed that signal fading caused by scintillation can increase the receiver tracking error.

The effects of receiver PLL tracking loop bandwidth tuning on scintillation monitoring have been discussed in the literature. Orus-Perez and Prieto-Cerdeira (2011) compared the scintillation indices observed by two different commercial scintillation monitoring receivers, that is, Novatel GSV4004B and Septentrio PolaRxS. Results showed that both receivers present comparable performance in scintillation monitoring. Rougerie et al. (2016) studied the effects of GNSS receiver PLL bandwidth tuning on scintillation indices calculation. They suggested that receiver tuning has almost no effect on *S*4 and *Phi*60 calculation. The cut-off frequency can affect the shape of the phase spectrum. However, these analyses only focus on scintillation indices estimation with different receivers or receiver tracking loop parameters. The effects of receiver tuning on tracking jitter estimation under scintillation are not considered.

To address the above limitation, a hardware simulator is used to generate GNSS signals affected by different levels of scintillation. An ionospheric scintillation monitoring receiver (ISMR) is connected to the simulator to record the GPS scintillation data. The scintillation indices and $C/N0$ observed for different tracking loop parameters are studied. The PLL tracking jitter is estimated using the theoretical models with receiver tuning. Discriminator output noise levels are calculated to verify the values of the estimated tracking jitters. This study focuses on (1) understanding the effects of receiver tuning on scintillation monitoring and tracking jitter estimation under scintillation; (2) verifying the relationship between the tracking jitters estimated by theoretical models and calculated by the PLL discriminator output. Novel approaches are also proposed to calculate the 1-s scintillation indices, which enables to estimate the jitter at 1-s intervals. Scintillation data processing and scintillation indices calculation are introduced next, followed by the description of PLL tracking loop models and tracking jitter estimation methods under scintillation. The experimental set up and scintillation data processing flow are then introduced. Results and discussions are provided next. Conclusions and remarks are given at the end.

2. Ionospheric Scintillation

The *S*4 and *Phi*60 indices are used to characterize amplitude and phase scintillation intensity, respectively, which relate to fluctuations in amplitude and phase of radio frequency signals caused by ionospheric irregularities. *S*4 is defined as the standard deviation of the detrended signal intensity normalized by its mean over 60 s (Van Dierendonck et al., 1993; Van Dierendonck, 1999):

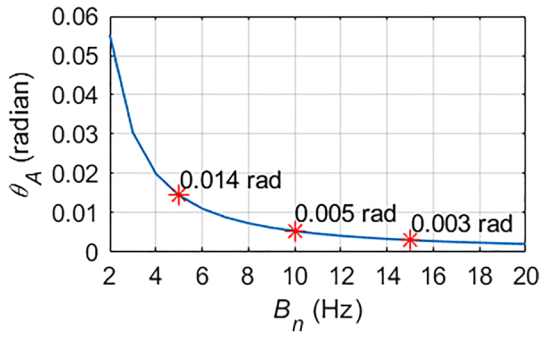

Figure 2. Oscillator noise induced tracking jitter θ_A in relation to B_n.

$$S4_{total} = \sqrt{\frac{\langle P_{det}^2 \rangle_{60s} - \langle P_{det} \rangle_{60s}^2}{\langle P_{det} \rangle_{60s}^2}}, \quad (1)$$

where P_{det} is the detrended signal intensity and $\langle \cdot \rangle$ denotes arithmetic mean. The intensity detrending is accomplished by applying a sixth-order low pass Butterworth filter to the measured intensity P, which is calculated by

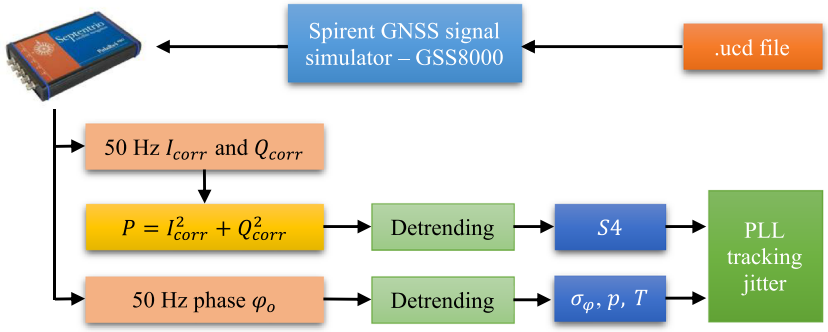

Figure 3. Experiment setup and data processing flow chart.

$$P = \sqrt{I_{corr}^2 + Q_{corr}^2}, \tag{2}$$

where I_{corr} and Q_{corr} are the 50 Hz post-correlation In-phase and Quadra-phase measurements, respectively. Readers interested in the intensity detrending process may refer to Van Dierendonck et al. (1993) and Van Dierendonck and Arbesser-Rastburg (2004) for more details.

As the ambient noise in the receiver also causes signal intensity fluctuation, the $S4_{\text{total}}$ calculated by Equation 1 needs to be corrected to remove the ambient noise contribution. According to Van Dierendonck et al. (1993), the ambient noise contribution is given by

$$S4_{noise} = \sqrt{\frac{100}{c/n_0}\left[1 + \frac{500}{19^{*}c/n_0}\right]}, \tag{3}$$

where c/n_0 is fractional form of $C/N0$, calculated by $c/n_0 = 10^{0.1^{*}C/N0}$. Thus, the corrected $S4$ is calculated as (Van Dierendonck et al., 1993)

$$S4 = \begin{cases} \sqrt{S4_{total}^2 - S4_{noise}^2} & if\ S4_{total} > S4_{noise} \\ 0 & if\ S4_{total} \le S4_{noise} \end{cases}. \tag{4}$$

The corrected $S4$ is employed to carry out the analysis in this study.

*Phi*60 is defined as the standard deviation of the detrended carrier phase measurements in 60 s, given by (Van Dierendonck, 1999)

$$Phi60 = \sqrt{\langle \varphi_{det}^2 \rangle_{60s} - \langle \varphi_{det} \rangle_{60s}^2}, \tag{5}$$

where φ_{det} is the detrended carrier phase. The detrending of the carrier phase measurements is realized by passing the high frequency carrier phase measurements through a sixth-order high pass Butterworth filter with a cut-off frequency of 0.1 Hz (Van Dierendonck et al., 1993; and reference therein).

Power spectral density (PSD) of the detrended carrier phase measurements in 1 min is calculated to characterize phase scintillation in the frequency domain. The temporal power spectrum of the detrended carrier phase is given by (Rino, 1979)

$$S_\varphi(f) = \frac{T}{\left[f^2 + f_0^2\right]^{p/2}}, \tag{6}$$

where f_0 is the frequency corresponding to the outer scale size of irregularities. p is the opposite of the slope of the line, that is fitted to the PSD in log-log axes over 0.1 to 25 Hz. T is the energy spectral

Table 1
Tracking Loop Configurations for Each Case in the Analysis

	B_n (Hz)	η (ms)	Scintillation effects
Case 1	5	10	Enabled
Case 2	10	10	Enabled
Case 3	15	10	Enabled
Case 4	15	20	Enabled
Case 5	15	10	Disabled

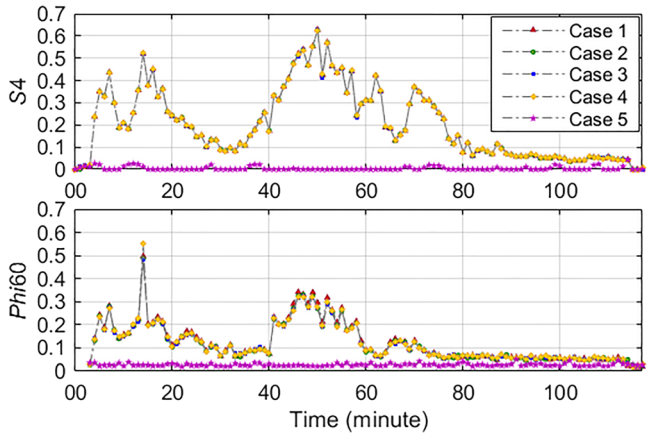

Figure 4. Variations of *S*4 (top) and *Phi*60 (bottom) in relation to time with different B_n and η.

density at 1 Hz, called spectral strength. When $f \gg f_0$, which is usually the practical case, $S_\varphi(f) \approx Tf^{-p}$. More details regarding the spectrum analysis of scintillation can be found in Yeh and Liu (1982) and Strangeways (2009).

According to Rino (1979), the carrier phase variance is estimated by integrating Equation 6 over all the frequencies. Thus, in the practical case, the phase variance is calculated by (Aquino et al., 2007; Conker et al., 2003; Rino, 1979)

$$\sigma_\varphi^2 = 2\int_{0.1}^{25} Tf^{-p}\mathrm{d}f. \tag{7}$$

Performing Equation 7, the following equation is obtained (Aquino et al., 2007):

$$\sigma_\varphi^2 = 2T\left[\frac{25^r - 0.1^r}{r}\right], \tag{8}$$

where $r = 1 - p$. Equation 8 presents the relationship among σ_φ, p, and T. If the PSD is calculated using 1-min detrended carrier measurements, σ_φ becomes the approximate of *Phi*60.

3. PLL Tracking Loop Models and Tracking Jitter Under Scintillation

The PLL tracking loop is implemented in coherent GNSS receivers to match the local replica of the received signal and to provide carrier phase measurements. A simplified linear PLL tracking loop model is demonstrated in Figure 1 (Gardner, 2005; Razavi et al., 2008; Van Dierendonck, 1996). The discriminator measures the tracking error $\Delta\varphi$, which is the difference between the incoming phase φ_i and the receiver locally duplicated phase φ_o. The output of the discriminator, denoted as δ_φ, is filtered by the loop filter $F(s)$. The output of $F(s)$ is then input to Number Controlled Oscillator to provide an updated φ_o, which feeds back to the tracking loop and matches with the incoming phase again (Braasch & Van Dierendonck, 1999; Kaplan & Hegarty, 2017).

The performance of the tracking loop is indicated by the tracking jitter, i.e., the standard deviation of the tracking error $\Delta\varphi$. The PLL tracking jitter under scintillation is given by (Conker et al., 2003; Knight & Finn, 1998)

$$\sigma_{\Delta\varphi} = \sqrt{\sigma_T^2 + \sigma_{pha}^2 + \theta_A^2}, \tag{9}$$

where σ_T^2 is the thermal noise component taking the amplitude scintillation into consideration. σ_{pha} is the phase scintillation induced tracking jitter. θ_A is the tacking jitter due to oscillator noise. Under amplitude scintillation, the thermal noise is enhanced in the tracking loop in relation to *S*4 levels. According to Conker et al. (2003), the tracking jitter thermal noise component under scintillation is evaluated as

$$\sigma_T^2 = \frac{B_n\left[1 + \dfrac{1}{2\eta c/n_0\left(1-2(S4)^2\right)}\right]}{c/n_0\left(1-(S4)^2\right)},\ S4 < \frac{\sqrt{2}}{2}, \tag{10}$$

where B_n and η are the PLL bandwidth and coherent integration time, which are essential parameters selected by the designer of the receiver tracking loop. The selection of B_n and η can affect the stability and sensitivity of the PLL in response to noise (Gardner, 2005). Equation 10 shows that σ_T^2 is a function of *S*4 and *C*/*N*0, as well as PLL B_n and η. It should be noted that the *C*/*N*0 here is the 60-s averaged value

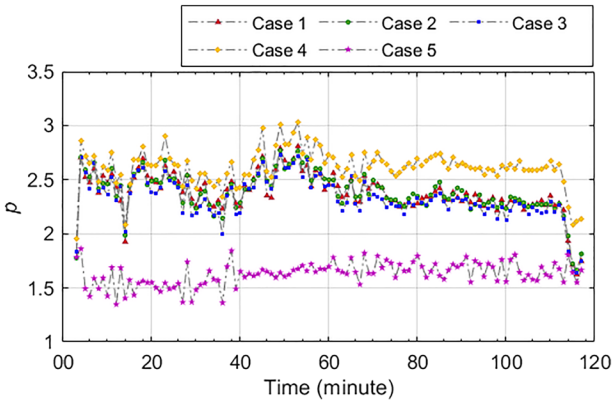

Figure 5. Variation of p values in relation to time with receiver tuning.

Table 2
Averaged p Values for Cases 1 to 5

	Case 1	Case 2	Case 3	Case4	Case 5
Averaged p	2.38	2.38	2.33	2.61	1.63

corresponding to the interval in which the scintillation index is calculated. When $S4$ is 0, Equation 10 becomes the standard thermal noise tracking error for carrier phase tracking, given by (Kaplan & Hegarty, 2017)

$$\sigma_t^2 = \frac{B_n}{c/n_0}\left[1 + \frac{1}{2\eta c/n_0}\right]. \tag{11}$$

The phase scintillation induced tracking jitter can be calculated through (Knight & Finn, 1998)

$$\sigma_{pha}^2 \approx \frac{\pi T}{k f_n^{p-1} \sin\left(\frac{[2k+1-p]\pi}{2k}\right)},\ 1 < p < 2k, \tag{12}$$

where k is the PLL loop order. f_n is the loop natural frequency.

θ_A is due to the instability of the oscillator in both the receiver and satellite clocks. As the GNSS satellites use a stable atomic clock, the satellite oscillator noise is ignorable. The receiver oscillator noise is constant for an individual receiver. According to Irsigler and Eissfeller (2002), for a third-order PLL, θ_A^2 is calculated by

$$\theta_A^2 = 2\pi^2 f_L^2 \left[\frac{\pi^2 h_{-2}}{3\omega_n^3} + \frac{\pi h_{-1}}{3\sqrt{3}\omega_n^2} + \frac{h_0}{6\omega_n}\right] (\text{rad}^2), \tag{13}$$

where f_L is the carrier frequency. h_{-2}, h_{-1}, and h_0 are clock parameters determined by the type of oscillator. The ISMR used in this study is implemented with an oven-controlled crystal oscillator. According to the clock parameters given by Irsigler and Eissfeller (2002), θ_A is calculated as a function of B_n on GPS L1 band, as Figure 2 shows. θ_A is seen to be much higher when B_n = 5 Hz compared with 10 and 15 Hz.

Equation 9 has been used in previous studies to evaluate the effect of scintillation on receiver tracking loops (Aquino et al., 2009; Sreeja et al., 2011; Strangeways et al., 2011; Vani et al., 2019). From Equations 9, 10, and 12, it can be known that the rate of scintillation indices determines the rate of the estimated tracking jitters.

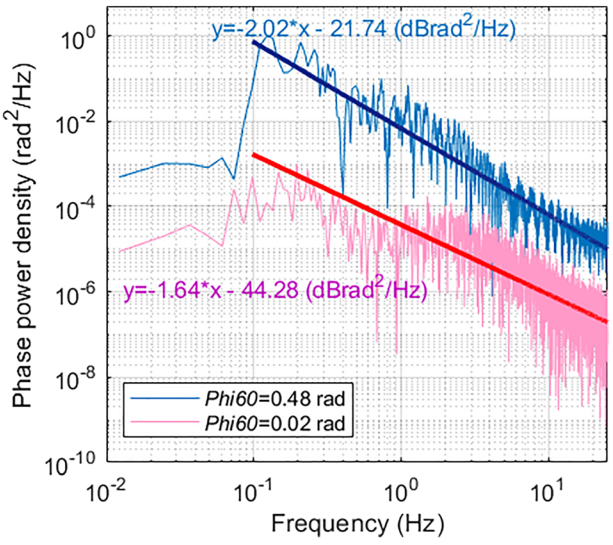

Figure 6. PSD curves of two typical minutes with and without scintillation with receiver default settings, i.e., B_n = 15 Hz and η = 10 ms.

The ISMR used in this analysis applies an arctangent discriminator. Thus, the PLL discriminator output is calculated as (Kaplan & Hegarty, 2017)

$$\delta_\varphi = \text{atan}\left(\frac{Q_{corr}}{I_{corr}}\right), \tag{14}$$

and the standard deviation of discriminator output noise is given by

$$\sigma_{\delta_\varphi} = \sqrt{\left\langle \delta_\varphi^2 \right\rangle - \left\langle \delta_\varphi \right\rangle^2}. \tag{15}$$

On the other hand, according to Razavi et al. (2008), the discriminator output noise is considered as the sum of thermal noise σ_w^2 and correlated noise σ_c^2, given by

$$\sigma_{\delta_\varphi} = \sqrt{\sigma_w^2 + \sigma_c^2}. \tag{16}$$

In this study, σ_c^2 is mainly due to the oscillator noise and scintillation effects. From Equation 16, σ_c is calculated by

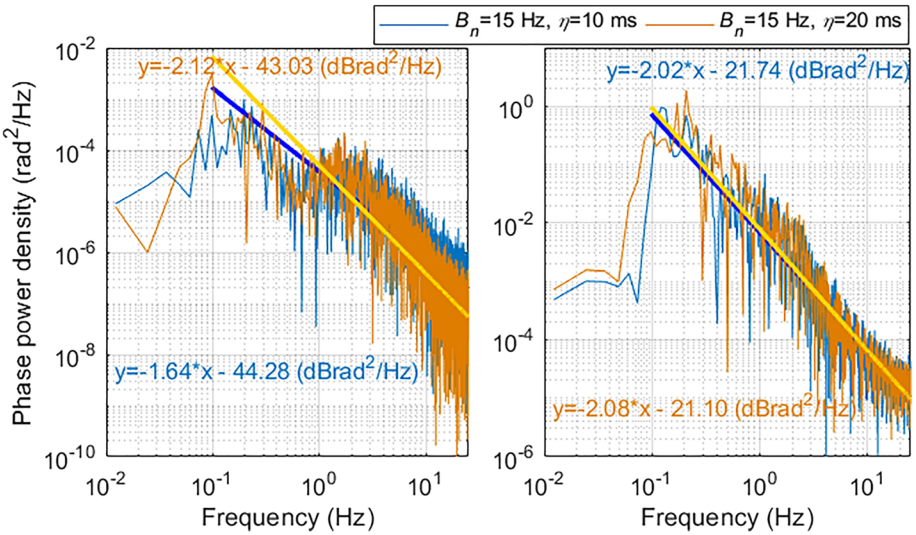

Figure 7. PSD curves of detrended carrier phase measurements with receiver tuning at 116th minute with *Phi*60 = 0.02 rad (left) and 14th minute with *Phi*60 = 0.48 rad (right).

$$\sigma_c = \sqrt{\sigma^2_{\delta_\varphi} - \sigma^2_w}. \tag{17}$$

It should be noted that the thermal noise in Equation 16 is the noise in the output of the discriminator, which is propagated through the closed-loop noise time-update function to the thermal noise in the tracking error variances, given by (Groves, 2013; Van Dierendonck et al., 1992)

$$\sigma^2_t \approx 2B_n\eta\sigma^2_w. \tag{18}$$

With Equations 16, 17, and 18, the tracking error can be estimated using the discriminator output by

$$\sigma_{\Delta\varphi\_discri} = \sqrt{\sigma^2_{\delta_\varphi} - \frac{\sigma^2_t}{2B_n\eta} + \sigma^2_t}. \tag{19}$$

Equation 19 offers an alternative way to estimate the PLL carrier phase tracking jitter. It can help to validate the values of the tracking jitter estimated using Equation 9.

4. Experimental Setup and Data Processing Flow

The experimental setup to generate scintillation data and data processing flow is described in this section. As Figure 3 shows, a Spirent GNSS signal simulator—GSS8000—available at the University of Nottingham is used to generate GPS L1 signals. A user command file (.ucd file) is activated in the simulation to superimpose scintillation effects on the signals. The .ucd file used in this study was generated from a 2-hr real life scintillation data set collected at Presidente Prudente, a low latitude scintillation monitoring station near the geomagnetic equator in Brazil. A Septentrio PolaRxS Pro receiver is connected to the GSS8000 simulator to record the simulated GPS L1 data. The PolaRxS receiver is a multifrequency multiconstellation receiver dedicated to ionospheric monitoring (www.septentrio.com/en/support/polarx/polarxs). The receiver can output 50 Hz I_{corr} and Q_{corr} measurements and carrier phase data. The tracking loop bandwidth and the coherent integration time of the receiver can be configured by the user through a friendly graphical user interface. In this

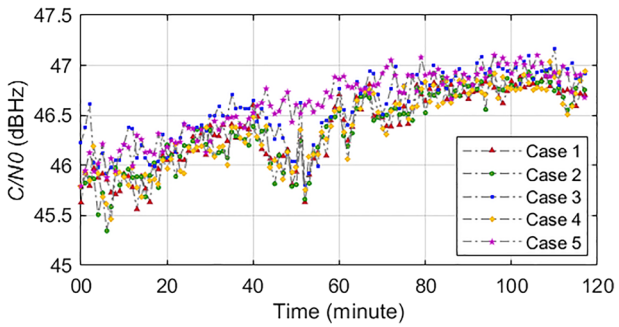

Figure 8. *C*/*N*0 variation as a function of time with receiver tuning.

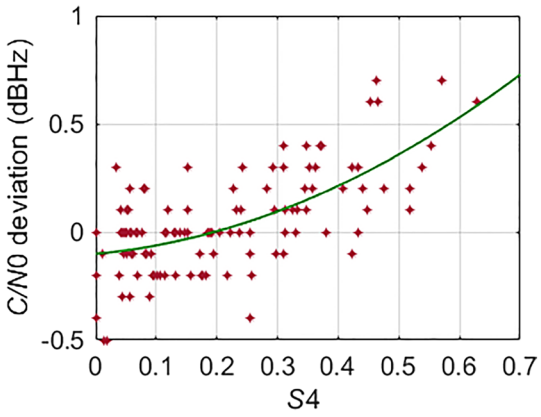

Figure 9. *C*/*N*0 deviations between signals in Cases 3 and 5 as a function of *S*4.

analysis, a total number of five simulations is carried out by configuring different B_n and η. The configurations of the tracking loop for each case are summarized in Table 1. It is worth mentioning that Case 3 has the same parameters as the default receiver configuration. Clean data are also generated in Case 5 for comparison. Additionally, when the .ucd file is activated in the simulation, the same scintillation scenario is applied to all the visible satellites. Therefore, only one satellite is selected for the analysis in this study.

The 50 Hz I_{corr} and Q_{corr} measurements logged by the receiver in each case are used to calculate the signal intensity, which is then detrended to calculate *S*4 in the analysis. The 50 Hz carrier phase measurements are detrended directly and *Phi*60, *p*, *T* are calculated thereafter. The PLL tracking jitter is finally estimated, and comparisons are made for different tracking loop parameters. It should be noted that the *C*/*N*0 values logged by the receiver are used to carry out the analysis in this work.

5. Scintillation Index Calculation With Receiver Tuning

The calculated amplitude and phase scintillation indices under different tracking loop bandwidths and coherent integration times are initially presented in this section. Figure 4 shows the variation of *S*4 and *Phi*60 in relation to time. From the figure, both *S*4 and *Phi*60 are seen to increase between the 5th and 20th minute and the 40th and 60th minute. The strongest amplitude scintillation occurs at the 50th minute when *S*4 is around 0.62, while the largest *Phi*60 is observed at the 14th minute, with a value of around 0.50 rad. Additionally, the *S*4 indices calculated with different B_n and η have few differences, which indicates that both loop bandwidth and integration time have almost no effect on *S*4 calculation. This agrees with the conclusions in Rougerie et al. (2016). Meanwhile, there are slight differences in *Phi*60 when B_n and η are different, especially when *Phi*60 is higher than 0.2 rad. In Case 5 when scintillation effects are not added in the signal simulation, both *S*4 and *Phi*60 show extremely low levels.

The phase scintillation spectral slope *p* is then calculated for different tracking loop bandwidths and integration times, as shown in Figure 5. When the signal is affected by scintillation, the values of *p* are generally higher than 2. Increases in *p* values can be seen with the increase in scintillation levels between the 40th and 60th minute. When η is configured to 10 ms, the *p* values of tracking loop with B_n of 5, 10, and 15 Hz are close, which means that the tracking loop bandwidth has low impacts on the *p* value estimation. By contrast, when integration time is increased to 20 ms, obvious higher values are seen, especially when scintillation levels are not strong between the 70th and 115th minute. Besides, *p* values are lower than 2 throughout in Case 5, which further suggests that the presence of scintillation can increase the *p* value. The averaged *p* values for each case are also summarized in Table 2. The effect of scintillation on the shape of the PSD curves and the calculation of *p* values will be explained in detail next.

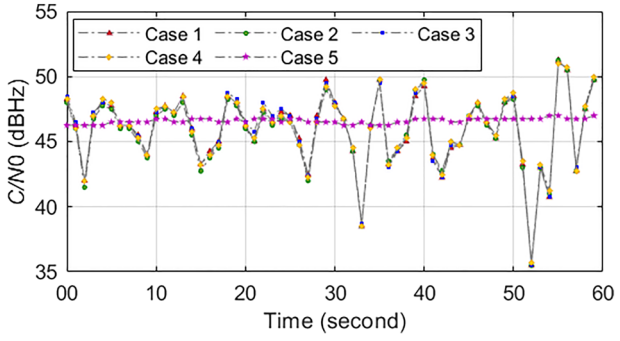

Figure 10. Comparison of 1-s *C*/*N*0 values with receiver tuning in the 51st minute with strong scintillation.

To further understand the effects of ionospheric scintillation and receiver tuning on signal carrier phase spectrum characteristics, the PSD of the detrended carrier phase measurements is studied. Figure 6 gives an example of the calculated PSD curves of two different minutes with receiver default settings, i.e., $B_n = 15$ Hz and $\eta = 10$ ms. The linear fitting functions of the PSD curves over 0.1 to 25 Hz in log-log axes are also included in the figure. As the figure shows, when there is no scintillation on the 116th minute, the phase power density curve, in pink, is relatively flat between 0.1 and 5 Hz. A large part of spectral energy is at high frequency. By contrast, when phase scintillation is present, as on the 14th minute, the PSD curve (in blue) obviously shifts upward resulting in an increased spectral energy. The spectral energy between 0.1 and 5 Hz also increases significantly, thus the curve has a steeper slope and a larger *p* value. It

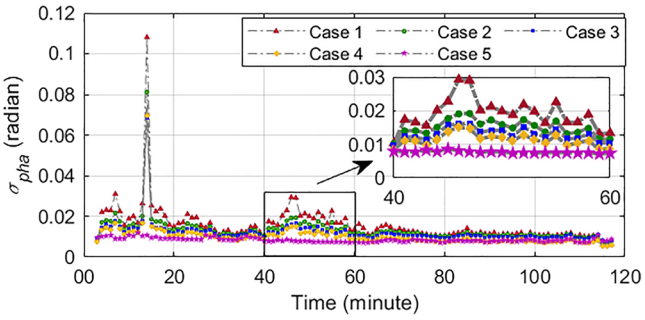

Figure 11. PLL phase scintillation induced tracking jitter σ_{pha} in relation to time with receiver tracking loop tuning.

should be noted that for both curves, the energy of the phase spectrum remains at a low level when the frequency is lower than 0.1 Hz. This is due to the effect of the high pass filter, which uses a cut-off frequency of 0.1 Hz.

Figure 5 shows that the p values are not significantly influenced by the change in PLL bandwidth. However, the increase in integration time can correspondingly increase the values of p. To analyze the impact of η on the calculation of p, the PSD curves on the 116th minute, when *Phi*60 is around 0.02 rad, and on the 14th minute, with *Phi*60 around 0.50 rad, are calculated with B_n set to 15 Hz and η set to 10 and 20 ms, respectively, as shown in Figure 7. When the scintillation effect is minor in the left panel, the PSD curves of both cases at low frequency are quite similar, while at high frequency, the spectrum energy is reduced by increasing the integration time from 10 to 20 ms. This results in a steeper slope of the fitted line between 0.1 and 25 Hz. However, on the right panel, the PSD curves of different integration times present similar patterns over all the frequency range, thus the slopes are close.

6. *C*/*N*0 Variation Under Scintillation

C/*N*0 is a crucial indicator of the signal strength and quality. According to Equation 11, the decrease in *C*/*N*0 can increase the thermal noise induced tracking jitter. In the presence of scintillation, particularly amplitude scintillation, *C*/*N*0 is attenuated to different extents due to the signal intensity fading (Seo et al., 2009), which further increases the tracking jitter. In this section, the *C*/*N*0 variation under scintillation with receiver tracking loop tuning is studied.

Figure 8 presents the receiver output *C*/*N*0 in relation to time with different tracking loop bandwidths and integration times. In the case of clean data, the *C*/*N*0 values, marked by magenta pentagrams, increase gradually as a function of time, which is due to the increase in satellite elevation, while when scintillation is present, downward tendencies are seen during scintillation occurrence. Thus, it can be concluded that amplitude scintillation can decrease the signal *C*/*N*0 levels to different extents. Additionally, *C*/*N*0 values in the figure are quite close to each other when the PLL is configured with different B_n and η, which means that receiver tuning has minor effects on signal *C*/*N*0 computation. It should be noted that the *C*/*N*0 values used here are the 1-min averaged value logged by the receiver.

C/*N*0 deviation between Case 3 and 5 can be calculated by

$$C/N0_{dev} = C/N0_{\text{case5}} - C/N0_{\text{case3}}. \tag{20}$$

In these two cases, both tracking loops refer to receiver default configurations, so that the difference in *C*/*N*0 is mainly caused by scintillation effects. Figure 9 shows the *C*/*N*0 deviations as a function of *S*4. It can be seen that when the scintillation level is weak, i.e., $S4 < 0.3$, the deviations are distributed near 0. However, with the increase in *S*4, the *C*/*N*0 deviation tends to increase, which further indicates the attenuation effects of amplitude scintillation on *C*/*N*0. A statistical model can be established to describe the relationship between *CN*0 decreases and *S*4 levels if there are enough samples. This will be part of future study.

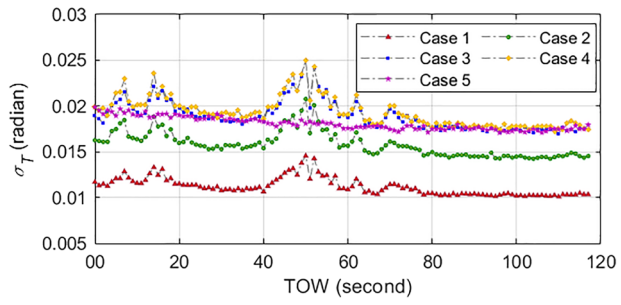

Figure 12. PLL jitter thermal noise component σ_T in relation to time with receiver tracking loop tuning.

As the 1-s *C*/*N*0 values are also available from the PolaRxS receiver outputs, the variation of *C*/*N*0 within 60 s, i.e., one scintillation event period, is analyzed. Figure 10 presents an example of the 1-s *C*/*N*0 output in the 51st minute, when strong scintillation occurs, with *S*4 reaching 0.63. As the figure shows, the *C*/*N*0 values of different tracking loop parameters under scintillation effects are quite similar, which again confirms that receiver tracking loop tuning would not significantly influence *C*/*N*0 calculation under scintillation. *C*/*N*0 values of the scintillation affected signals fluctuate dramatically within 1 min. The highest *C*/*N*0 is more than 50 dBHz, which is

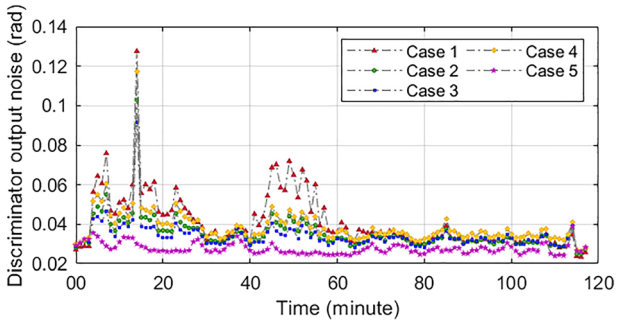

Figure 13. Variation of the standard deviation of discriminator output noise in relation to time.

much higher than the average value which is around 46 dBHz. Meanwhile, the $C/N0$ can be as low as almost 35 dBHz, which is far lower than the nominal values and will probably cause serious receiver tracking problems. On the contrary, in the case when clean data is simulated, the $C/N0$ remains relative stable around 46 dBHz over the whole minute. Thus, it can be seen that using 1-min averaged $C/N0$ to represent the signal strength and quality under scintillation is not accurate enough. The signal intensity may change significantly within 1 min.

7. Estimated PLL Tracking Jitters

The previous sections analyzed how the receiver tracking loop tuning affects scintillation indices calculation. In this section, the estimation of the PLL tracking jitter using Equation 9 with different tracking loop bandwidths and integration times is presented. It should be noted that, as θ_A is considered to be constant once the tracking loop bandwidth is defined, only the analyses of σ_{pha} and σ_T are presented in this section.

The evaluated PLL σ_{pha} and σ_T under scintillation are shown in Figure 11. For comparison, the tracking jitter of clean signals (Case 5) is also included. It can be seen from the figure that σ_{pha} is generally at low levels in all cases, except for one epoch at the 14th minute when *Phi*60 suddenly jumps to 0.5 rad and σ_{pha} exceeds 0.06 rad in the first four cases. Thus, it might be concluded that phase scintillation will not cause serious tracking problems for most PLL settings when *Phi*60 < 0.4 rad. A sudden increase of *Phi*60 may cause extremely large tracking errors. This conclusion needs to be further verified by carrying out more experiments with stronger phase scintillation events. Additionally, when the receiver PLL bandwidth increases from 5 to 15 Hz, σ_{pha} decreases gradually, although the difference is slight. The tracking loop when B_n is set to 5 Hz has the largest σ_{pha}. This indicates that the tracking loop with lower bandwidth is more susceptible to phase scintillation, which is in agreement with the conclusions by Knight and Finn (1998). Furthermore, it can be seen from the figure that in general, the increase in tracking loop integration time can slightly decrease the phase induced tracking jitter, as the σ_{pha} in Case 4 is slightly lower than that of Case 3 where η is set to 10 ms.

The estimated σ_T in each case is shown in Figure 12. With different loop bandwidths, the thermal noise jitter is generally at different levels, but following similar patterns. Obvious increases in σ_T can be seen when scintillation becomes stronger. The PLL with B_n of 5 Hz presents the smallest jitter over the whole period, even

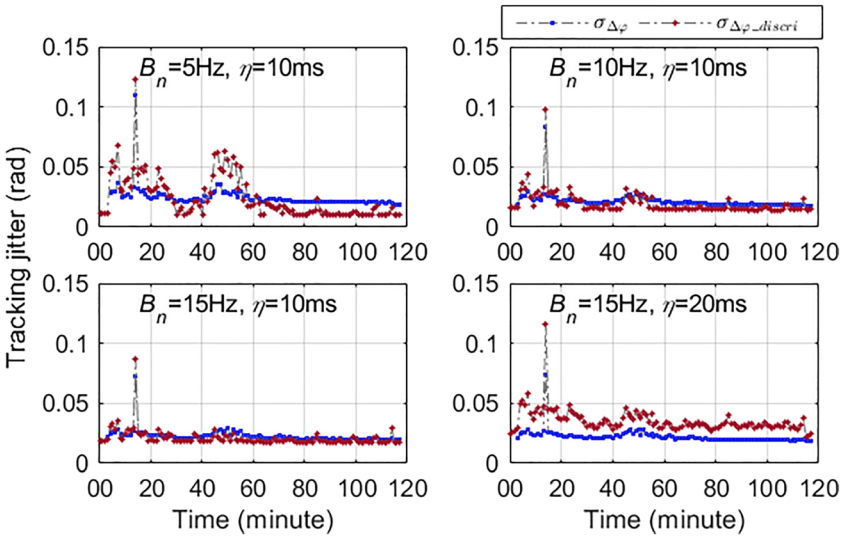

Figure 14. Variation of PLL of $\sigma_{\Delta\varphi}$ and $\sigma_{\Delta\varphi\_discri}$ with receiver tracking loop tuning.

Table 3
RMS of the Difference and Correlation Coefficients Between $\sigma_{\Delta\varphi}$ and $\sigma_{\Delta\varphi\_discri}$ Shown in Figure 14

	Case 1	Case 2	Case 3	Case 4
RMS (rad)	0.0123	0.0047	0.0037	0.0142
Correlation coefficient	0.80	0.93	0.92	0.92

lower than that of the clean data of Case 5, while the largest values are seen on the tracking loop with B_n = 15 Hz. This is reasonable as σ_T is proportional to B_n, as defined in Equation 11. Additionally, it can be seen that the values of σ_T in Cases 3 and 4 are quite close, which means that the integration time has a minor effect on the tracking loop jitter.

As a result, a smaller B_n will decrease the value of σ_T. But this has an opposite effect for phase scintillation induced tracking jitter and oscillator noise, because both will increase with the decrease in B_n. Therefore, there is a trade-off when selecting the PLL bandwidth in order to maximize the receiver performance in the presence of scintillation.

8. PLL Tracking Jitter Validation Using the Discriminator Output

High frequency I_{corr} and Q_{corr} measurements are not output by most commercial and generic receivers. Therefore, Equation 9 is commonly used to estimate the effect of scintillation on the PLL tracking performance. Equation 19 offers an alternative way to estimate the PLL carrier phase tracking jitter. In this study, the ISMR is capable of outputting 50 Hz I_{corr} and Q_{corr} data in the predetection integration process, which makes it possible to verify the values of tracking jitter estimated by Equation 9 using discriminator output errors.

Figure 13 first presents the variation of σ_{δ_φ} calculated using Equation 15 in relation to time. As the figure shows, σ_{δ_φ} increases to different extents in each case during the scintillation period. The largest value is seen on the 14th minute when both *S*4 and *Phi*60 are at high levels. Additionally, σ_{δ_φ} in Case 1 is generally higher when scintillation occurs, followed by that in Cases 2 and 3, which means the increase in B_n can decrease the total discriminator output noise variance and improve the receiver tracking performance in the presence of scintillation. Furthermore, σ_{δ_φ} in Case 4 is slightly higher than that in Case 3, indicating that a larger η may decrease the tracking loop jitter. This needs to be further verified with more scintillation events.

To validate the estimated tracking jitter using Equation 9, $\sigma_{\Delta\varphi\_discri}$ is calculated using the discriminator output noise. Figure 14 shows the variation of $\sigma_{\Delta\varphi}$ and $\sigma_{\Delta\varphi\_discri}$ with receiver tuning. The correlation coefficients along with the Root-Mean-Square (RMS) of the difference between $\sigma_{\Delta\varphi}$ and $\sigma_{\Delta\varphi\_discri}$ are calculated and summarized in Table 3. It can be seen that for all the four cases, $\sigma_{\Delta\varphi}$ follows the pattern of $\sigma_{\Delta\varphi\_discri}$, although there are slight biases between $\sigma_{\Delta\varphi}$ and $\sigma_{\Delta\varphi\_discri}$. The total estimated tracking jitters $\sigma_{\Delta\varphi}$ in Cases 1, 2, and 3 are generally higher than $\sigma_{\Delta\varphi\_discri}$ over the whole period, except in Case 1 when $\sigma_{\Delta\varphi\_discri}$ overtakes $\sigma_{\Delta\varphi}$ during the scintillation occurrence. The RMSs of the differences for Cases 2 and 3 are less than 0.01 rad. In Case 4, $\sigma_{\Delta\varphi}$ is seen lower than $\sigma_{\Delta\varphi\_discri}$ during all the period. The RMS of the difference is 0.0142 rad in this case, indicating that the increase in PLL integration time could result in underestimating the tracking jitter using Equation 9. Additionally, $\sigma_{\Delta\varphi}$ and $\sigma_{\Delta\varphi\_discri}$ are seen to be highly correlated for these four cases. Obvious increases are seen during the scintillation occurrence. This means both of $\sigma_{\Delta\varphi}$ and $\sigma_{\Delta\varphi\_discri}$ are sensitive to scintillation effects. Moreover, the estimated tracking jitter $\sigma_{\Delta\varphi}$ is seen to be more stable than $\sigma_{\Delta\varphi\_discri}$ in all the cases. The explanation may be that when estimating the tracking jitter, Equation 10 uses the 1-min averaged $C/N0$, therefore not accounting for the $C/N0$ fluctuations within 1 min in the calculation, while, for the calculation of $\sigma_{\Delta\varphi\_discri}$ based on I_{corr} and Q_{corr}, every measurement is taken into account. The variation of $C/N0$ within 1 min is thus reflected.

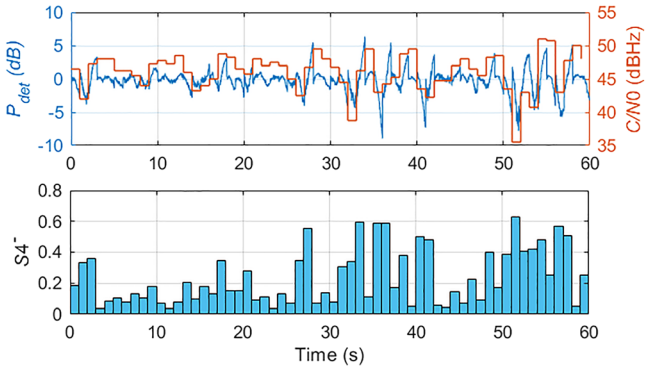

Figure 15. Variation of the detrended signal intensity, $C/N0$ (top) and 1-s amplitude scintillation index $S4^{-}$ (bottom) in the 51st minute of Case 3.

In order to further verify the relationship between $\sigma_{\Delta\varphi}$ and $\sigma_{\Delta\varphi\_discri}$ at a rate of 1 s, the 1-s tracking jitter and discriminator noise are calculated. The 1-s σ_{δ_φ} is easy to obtain by using Equation 15 at 1 s intervals, whereas, to estimate tracking jitter $\sigma_{\Delta\varphi}$ using Equation 9 at a

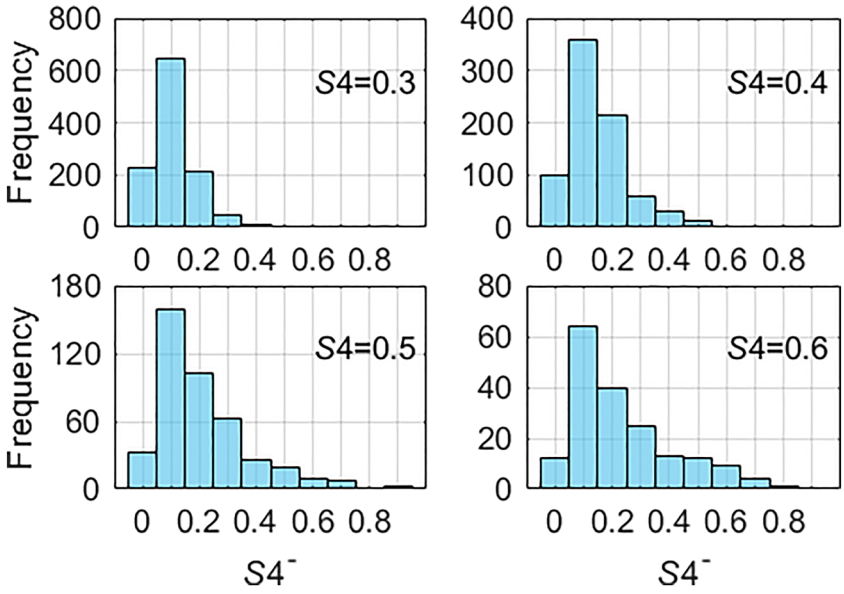

Figure 16. Histograms of 1-s $S4^{-}$ as a function of 1-min $S4$ when it equals to 0.3, 0.4, 0.5, and 0.6 in Case 3.

rate of 1 s, 1-s scintillation indices are required. Therefore, the following approaches are proposed in this study to calculate the 1-s scintillation indices:

1. The 1-s amplitude scintillation index, denoted as $S4^{-}$, is calculated using the same data processing method for the calculation of $S4$, except that the normalization is performed within 1 s. Then, σ_T is computed using Equation 10 with the $S4^{-}$ and 1-s $C/N0$ output by the receiver.
2. With 50 Hz carrier phase measurements, there are not enough number of samples to calculate the phase PSD in 1 s, thus the p and T indices for phase scintillation cannot be evaluated according to the approaches described in section 2. According to Aquino et al. (2007), the 1-hr averaged spectral slope p can lead to values of T in close agreement with those estimated by 1-min discrete of p. Additionally, the 1-s σ_φ can be estimated using 50 Hz detrended carrier measurements. Thus, with the hourly averaged p, 1-s T can be estimated using Equation 8. The 1-s σ_{pha} is consequently calculated using the estimated p and T at a rate of 1 s.

Figure 15 shows the 1-s amplitude scintillation index in the 51st minute of Case 3. It can be seen from the top panel that the signal intensity and $C/N0$ fluctuate significantly within the minute. The difference between the maximum and minimum $C/N0$ can be as large as 15 dBHz, indicating the severe effects of amplitude scintillation on signal quality. The 1-s amplitude scintillation index $S4^{-}$ in the bottom panel shows the levels of signal fluctuations in each second. When the signal intensity suffers from dramatic variations, e.g., on the 33rd, 35th, 51st second, $S4^{-}$ increases correspondingly. The largest $S4^{-}$ and minimum $C/N0$ both occur on the 51st second with $S4^{-} = 0.62$ and $C/N0 = 35.5$ dBHz.

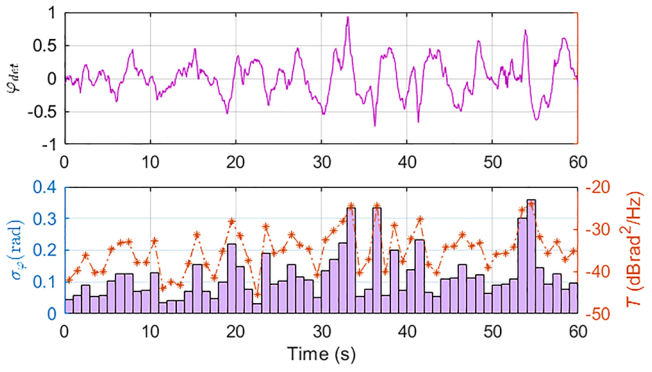

Figure 17. Variation of the detrended signal carrier phase (top) and 1-s phase scintillation indices σ_φ and T (bottom) in the 51st minute of Case 3.

Figure 16 shows the histograms of 1-s $S4^{-}$ samples as a function of 1-m $S4$ when it equals to 0.3, 0.4, 0.5, and 0.6 in Case 3. It can be seen that for all these four levels of $S4$, the 1-s amplitude scintillation index with $S4^{-} = 0.1$ has the largest frequency. When $S4$ is 0.5 or 0.6, most values of $S4^{-}$ are less than 0.4, which indicates that even when $S4$ shows the moderate levels of scintillation, there are large parts of weak scintillation within the $S4$ calculation period.

The 1-s phase scintillation σ_φ and T as well as the variation of the detrended carrier phase measurements in the 51st minute of Case 3 are presented in Figure 17. The detrended carrier phase in the top

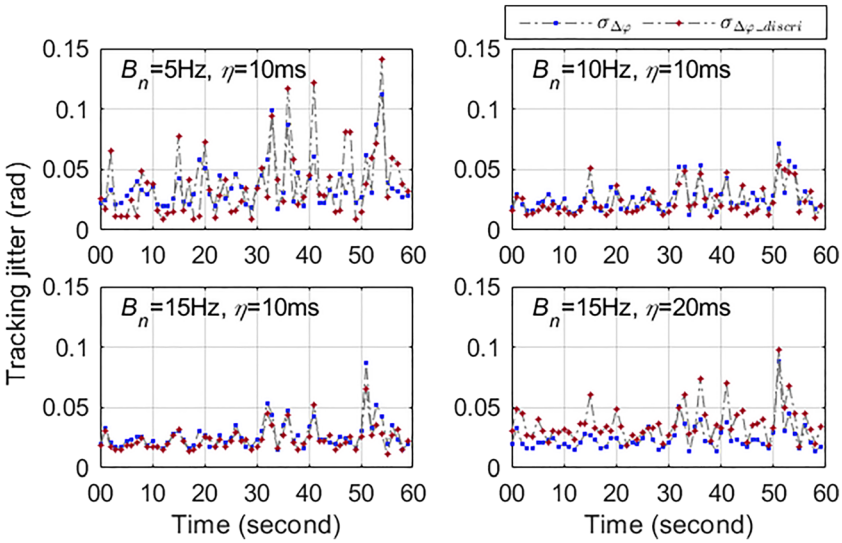

Figure 18. Variations of 1-s $\sigma_{\Delta\varphi}$ and $\sigma_{\Delta\varphi\_discri}$ with receiver tuning under scintillation effects in the 51st minute of Case 3.

panel is seen to vary rapidly, leading to the increases in both 1-s σ_φ and T indices. σ_φ and T present good correlation within this minute. The largest σ_φ and T indices are both seen on the 54th second. The 1-s scintillation indices are used to further calculate the 1-s tracking jitters, which is shown thereafter.

The variations of the 1-s $\sigma_{\Delta\varphi}$ and $\sigma_{\Delta\varphi\_discri}$ in the 51st minute of Case 3 are shown in Figure 18. As it can be seen from the figure, tracking jitter shows more fluctuations compared with Figure 14—this is because that using 1-s scintillation indices and $C/N0$ to calculate the tracking jitters can reflect more details of the signal fluctuations under scintillation. The values of $\sigma_{\Delta\varphi}$ and $\sigma_{\Delta\varphi\_discri}$ are seen to be closer and to follow similar patterns. In Case 4, when B_n is 15 Hz and η is 20 ms, $\sigma_{\Delta\varphi}$ is seen to be less than $\sigma_{\Delta\varphi\_discri}$ over the corresponding period of time, which is in agreement with the results shown in Figure 14. The increases in $\sigma_{\Delta\varphi}$ and $\sigma_{\Delta\varphi\_discri}$ are directly related to the increase of signal fluctuation, which is also represented by the scintillation indices in Figures 15 and 17. In Cases 2, 3, and 4, the largest $\sigma_{\Delta\varphi}$ and $\sigma_{\Delta\varphi\_discri}$ is seen on the 51st second, when exactly the largest $S4^-$ and minimum $C/N0$ occurs. However, in Case 1, the largest $\sigma_{\Delta\varphi}$ and $\sigma_{\Delta\varphi\_discri}$ is seen on the 54th second, when strong phase scintillation occurs. This further verifies that tracking loop with lower bandwidth is more susceptible to phase scintillation.

The RMS of the difference and correlation coefficients between $\sigma_{\Delta\varphi}$ and $\sigma_{\Delta\varphi\_discri}$ for each case shown in Figure 18 are summarized in Table 4. The theoretical tracking jitter $\sigma_{\Delta\varphi}$ in Cases 2 and 3 presents the relatively close values to $\sigma_{\Delta\varphi\_discri}$, with RMS of the difference less than 0.01 rad. Additionally, $\sigma_{\Delta\varphi}$ is seen to highly correlate with $\sigma_{\Delta\varphi\_discri}$ for all the cases, which means that both $\sigma_{\Delta\varphi}$ and $\sigma_{\Delta\varphi\_discri}$ are sensitive to the tracking errors caused by scintillation. Thus, it can be concluded that when high frequency post-correlation I_{corr} and Q_{corr} measurements are available, the value of $\sigma_{\Delta\varphi\_discri}$ can be used to verify the values of tracking jitters estimated using Equation 9 under scintillation. Moreover, the 1-s scintillation indices and tracking jitters can successfully represent the signal fluctuation under scintillation and tracking loop performance. More details of the signal distortion caused by scintillation can be reflected compared with the tracking jitter calculated every 1 min. However, there are still differences between $\sigma_{\Delta\varphi}$ and $\sigma_{\Delta\varphi\_discri}$, especially when PLL bandwidth is set to 5 Hz. Therefore, more advanced models need to be

Table 4
RMS of the Difference and Correlation Coefficients Between $\sigma_{\Delta\varphi}$ and $\sigma_{\Delta\varphi\_discri}$ Shown in Figure 18

	Case 1	Case 2	Case 3	Case 4
RMS (rad)	0.0216	0.0090	0.0063	0.0151
Correlation coefficient	0.68	0.74	0.90	0.80

developed to better account for scintillation effects on the GNSS receiver tracking loops. This will be the focus of the future work.

9. Conclusions and Remarks

This work analyzes the effects of receiver tracking loop tuning on ionospheric scintillation monitoring and PLL tracking jitter estimation. A hardware signal simulator is used to generate GPS scintillation data, which is recorded by a Septentrio ISMR. The following conclusions can be drawn based on the analysis:

1. By investigating the effects of receiver tuning on scintillation monitoring, it is found that $S4$ is less affected by both loop bandwidth and integration time, while for *Phi*60, very slight differences are seen with different loop configurations. When scintillation effects are minor, a large part of the spectral power is at high frequency, while, in the presence of scintillation, the spectral energy between 0.1 and 5 Hz increases significantly. Therefore, the phase PSD curve has a steeper slope. Additionally, the results show that p values are not related to the PLL bandwidth. However, the increase in PLL tracking loop integration time can correspondingly increase the values of p.
2. In the study of $C/N0$ variation under scintillation, $C/N0$ present quite similar values when PLL is configured with different tracking loop parameters, which leads to conclude that receiver tuning has minor effects on signal $C/N0$ computation under scintillation. By comparing the $C/N0$ differences between scintillation affected and clean signals, it is found that $C/N0$ deviation tends to increase with the increase in $S4$. A model can be established to describe the relationship between $C/N0$ and $S4$ levels with more scintillation data samples. This will be part of future study. The variation of 1-s $C/N0$ within 60 s is analyzed under strong amplitude scintillation. $C/N0$ values are seen to fluctuate dramatically. Thus, the conclusion can be drawn that using 1-min averaged $C/N0$ to represent the signal strength and quality under scintillation is not accurate enough as the signal may change significantly within 1 min.
3. By studying the estimated tracking jitter with receiver tracking loop tuning, it is found that the increase in PLL bandwidth can decrease the levels of σ_{pha}. This indicates that the tracking loop with lower bandwidth is more susceptible to phase scintillation. However, σ_T increases with the increase in B_n. Therefore, there is a trade-off when selecting the tracking loop bandwidth in order to maximize the receiver performance in the presence of scintillation.
4. By comparing the 1-min theoretically estimated tracking jitter $\sigma_{\Delta\varphi}$ and the tracking jitter $\sigma_{\Delta\varphi\_discri}$ estimated using the discriminator output noise, it is seen that $\sigma_{\Delta\varphi}$ is approximately close to $\sigma_{\Delta\varphi\_discri}$ although there are slight biases. In order to calculate tracking jitter at a rate of 1 s, new approaches are proposed to estimate the tracking jitter at 1-s intervals. The results show that 1-s scintillation indices and tracking jitters can successfully represent the signal fluctuation under scintillation and tracking loop performance. More details of the signal distortion caused by scintillation can be reflected compared with the tracking jitter calculated every 1 min. Additionally, the values of 1-s $\sigma_{\Delta\varphi}$ are seen to approximately match $\sigma_{\Delta\varphi\_discri}$, except when $B_n = 5$ Hz. This may be due to the fact that the theoretical equations in Conker et al. (2003) are not performing well with low loop bandwidth. More advanced models need to be developed to better account for scintillation effects on the GNSS receiver tracking loops. This will be the focus of the future work.

This study provides a better understanding of the receiver tuning effects on ionospheric scintillation monitoring and tracking jitter estimation. It can be of assistance for developing scintillation sensitive tracking error models. The study is also of great significance for GNSS receiver design to mitigate scintillation effects.

Acknowledgments

The author thanks the TREASURE project (www.treasure-gnss.eu), which received funding from the European Union's Horizon 2020 research and innovation programme under the Marie Skłodowska-Curie grant agreement 722023. Data from the Presidente Prudente station in Brazil is part of the CIGALA/CALIBRA network (http://ismrquerytool.fct.unesp.br/is/index.php). Monitoring stations from the network were deployed in the context of the Projects CIGALA and CALIBRA, both funded by the European Commission (EC) in the framework of the FP7-GALILEO-2009-GSA and FP7–GALILEO–2011–GSA–1a, respectively, and FAPESP Project Number 06/04008-2. The author also wants to thank Jean-Marie Sleewaegen from Septentrio Satellite Navigation, Chris Hill and Lei Yang from Nottingham Geospatial Institute for the helpful discussion. The User Command file (.ucd) used in this study to simulate scintillation data is available online (https://rdmc.nottingham.ac.uk/handle/internal/7023). Readers interested may use this file to simulate scintillation data following the process described therein.

References

Aarons, J. (1982). Global morphology of ionospheric scintillations. *Proceedings of the IEEE*, *70*(4), 360–378. https://doi.org/10.1109/PROC.1982.12314

Aquino, M., Andreotti, M., Dodson, A., & Strangeways, H. (2007). On the use of ionospheric scintillation indices as input to receiver tracking models. *Advances in Space Research*, *40*(3), 426–435. https://doi.org/10.1016/j.asr.2007.05.035

Aquino, M., Monico, J. F. G., Dodson, A. H., Marques, H., De Franceschi, G., Alfonsi, L., et al. (2009). Improving the GNSS positioning stochastic model in the presence of ionospheric scintillation. *Journal of Geodesy*, *83*(10), 953–966. https://doi.org/10.1007/s00190-009-0313-6

Basu, S., MacKenzie, E., & Basu, S. (1988). Ionospheric constraints on VHF/UHF communications links during solar maximum and minimum periods. *Radio Science*, *23*(3), 363–378. https://doi.org/10.1029/RS023i003p00363

Braasch, M. S., & Van Dierendonck, A. J. (1999). GPS receiver architectures and measurements. *Proceedings of the IEEE*, *87*(1), 48–64.

Conker, R. S., El-Arini, M. B., Hegarty, C. J., & Hsiao, T. (2003). Modelling the effects of ionospheric scintillation on GPS/satellite-based augmentation system availability. *Radio Science*, *38*(1), 1001. https://doi.org/10.1029/2000RS002604

Gardner, F. M. (2005). *Phaselock techniques*. Hoboken, NJ: John Wiley & Sons.

Groves, P. D. (2013). *Principles of GNSS, inertial, and multisensor integrated navigation systems*, Boston & London: Artech House.

Guo, K., Aquino, M., & Vadakke, V. S. (2019). Ionospheric scintillation intensity fading characteristics and GPS receiver tracking performance at low latitudes. *GPS Solutions*, *23*(2), 43. https://doi.org/10.1007/s10291-019-0835-1

Guo, K., Aquino, M., Veettil, S. V., Liu, Z., Chen, W., & Marques, H. A. (2019). *Analysis of ionospheric scintillation and its impact on PPP at low latitudes* (pp. 835–845). Paper presented at Proceedings of the ION 2019 Pacific PNT Meeting. https://doi.org/10.33012/2019.16842

Hegarty, C., El-Arini, M. B., Kim, T., & Ericson, S. (2001). Scintillation modelling for GPS-wide area augmentation system receivers. *Radio Science*, *36*(5), 1221–1231. https://doi.org/10.1029/1999RS002425

Humphreys, T. E., Psiaki, M. L., & Kintner, P. M. (2010). Modeling the effects of ionospheric scintillation on GPS carrier phase tracking. *IEEE Transactions on Aerospace and Electronic Systems*, *46*(4), 1624–1637. https://doi.org/10.1109/TAES.2010.5595583

Irsigler, M., & Eissfeller, B. (2002). PLL tracking performance in the presence of oscillator phase noise. *GPS Solutions*, *5*(4), 45–57. https://doi.org/10.1007/PL00012911

Kaplan, E., & Hegarty, C. (2017). *Understanding GPS: Principles and applications*. Boston & London: Artech House.

Knight, M., & Finn, A. (1998). *The effects of ionospheric scintillations on GPS* (pp. 673?685). Paper presented at Proceedings of the 11th International Technical Meeting of the Satellite Division of The Institute of Navigation (ION GPS 1998), Nashville, TN.

Moraes, A., Costa, E., de Paula, E. R., Perrella, W. J., & Monico, J. F. G. (2014). Extended ionospheric amplitude scintillation model for GPS receivers. *Radio Science*, *49*, 315–329. https://doi.org/10.1002/2013RS005307

Orus-Perez, R., & Prieto-Cerdeira, R. (2011). *Evaluation and calibration of GNSS receivers for ionospheric delay and scintillation measurements* (pp. 626–633). Paper presented at Proceedings of the 24th International Technical Meeting of the Satellite Division of The Institute of Navigation (ION GNSS 2011), Oregon Convention Center, Portland, OR.

Pi, X., Iijima, B. A., & Lu, W. (2017). Effects of ionospheric scintillation on GNSS-based positioning. *Journal of the Institute of Navigation*, *64*(1), 3–22. https://doi.org/10.1002/navi.182

Razavi, A., Gebre-Egziabher, D., & Akos, D. M. (2008). Carrier loop architectures for tracking weak GPS signals. *IEEE Transactions on Aerospace and Electronic Systems*, *44*(2), 697–710. https://doi.org/10.1109/TAES.2008.4560215

Rino, C. L. (1979). A power law phase screen model for ionospheric scintillation: 1. Weak scatter. *Radio Science*, *14*(6), 1135–1145. https://doi.org/10.1029/RS014i006p01135

Rougerie, S., Ait-Ighil, M., & Fabbro, V. (2016). Paper presented at Proceedings of the 29th International Technical Meeting of the Satellite Division of The Institute of Navigation (ION GNSS+ 2016), Oregon Convention Center, Portland, OR. *Impact of GNSS receiver tuning on the estimation of scintillation index* (pp. 1664–1671). https://doi.org/10.33012/2016.14769

Seo, J., Walter, T., Chiou, T. Y., & Enge, P. (2009). Characteristics of deep GPS signal fading due to ionospheric scintillation for aviation receiver design. *Radio Science*, *44*, RS0A16. https://doi.org/10.1029/2008RS004077

Sreeja, V., Aquino, M., & Elmas, Z. G. (2011). Impact of ionospheric scintillation on GNSS receiver tracking performance over Latin America: Introducing the concept of tracking jitter variance maps. *Space Weather*, *9*, S10002. https://doi.org/10.1029/2011SW000707

Strangeways, H. J. (2009). Determining scintillation effects on GPS receivers. *Radio Science*, *44*, RS0136. https://doi.org/10.1029/2008RS004076

Strangeways, H. J., Ho, Y. H., Aquino, M. H. O., Elmas, Z. G., Marques, H. A., Monico, J. F. G., & Silva, H. A. (2011). On determining spectral parameters, tracking jitter, and GPS positioning improvement by scintillation mitigation. *Radio Science*, *46*, RS0D15. https://doi.org/10.1029/2010RS004575

Vadakke Veettil, S., Aquino, M., Spogli, L., & Cesaroni, C. (2018). A statistical approach to estimate Global Navigation Satellite Systems (GNSS) receiver signal tracking performance in the presence of ionospheric scintillation. *Journal of Space Weather and Space Climate*, *8*(2018), A51. https://doi.org/10.1051/swsc/2018037

Van Dierendonck, A. J. (1996). GPS receivers. In B. W. Parkinson, & J. J. Spilker, Jr. (Eds.), *Global Positioning System: Theory and Applications* (Vol. 1, pp. 329–408). Washington, DC: AIAA.

Van Dierendonck, A. J. (1999). Eye on the ionosphere: Measuring ionospheric scintillation effects from GPS signals. *GPS Solutions*, *2*(4), 60–63. https://doi.org/10.1007/PL00012769

Van Dierendonck, A. J., & Arbesser-Rastburg, B. (2004). *Measuring ionospheric scintillation in the equatorial region over Africa, including measurements from SBAS geostationary satellite signals* (pp. 316–324). Paper presented at Proceedings of the 17th International Technical Meeting of the Satellite Division of The Institute of Navigation (ION GNSS 2004), Long Beach Convention Center, Long Beach, CA.

Van Dierendonck, A. J., Fenton, P., & Ford, T. (1992). Theory and performance of narrow correlator spacing in a GPS receiver. *Navigation*, *39*(3), 265–283. https://doi.org/10.1002/j.2161-4296.1992.tb02276.x

Van Dierendonck, A. J., Klobuchar, J., & Hua, Q. (1993). *Ionospheric scintillation monitoring using commercial single frequency C/A code receivers* (Vol. *93*, pp. 1333–1342). Paper presented at Proceedings of the 6th International Technical Meeting of the Satellite Division of The Institute of Navigation (ION GPS 1993), Salt Palace Convention Center, Salt Lake City, UT.

Vani, B. C., Forte, B., Monico, J. F. G., Skone, S., Shimabukuro, M. H., de Oliveira Moraes, A., et al. (2019). A novel approach to improve GNSS Precise Point Positioning during strong ionospheric scintillation: Theory and demonstration. *IEEE Transactions on Vehicular Technology*, *68*(5), 4391–4403. https://doi.org/10.1109/TVT.2019.2903988

Yeh, K. C., & Liu, C. (1982). Radio wave scintillations in the ionosphere. *Proceedings of the IEEE*, *70*(4), 324–360. https://doi.org/10.1109/PROC.1982.12313